Composition- and Shape-Controlled Synthesis and Optical Properties of ZnxCd1−xS Alloyed Nanocrystals

ARTICLE *in* ADVANCED FUNCTIONAL MATERIALS · MARCH 2005

Impact Factor: 11.81 · DOI: 10.1002/adfm.200400320

5 AUTHORS, INCLUDING:

Yunchao Li
Beijing Normal University
41 PUBLICATIONS **1,244** CITATIONS
SEE PROFILE

Mingfu Ye
Anhui University of Technology
26 PUBLICATIONS **801** CITATIONS
SEE PROFILE

Composition- and Shape-Controlled Synthesis and Optical Properties of $Zn_xCd_{1-x}S$ Alloyed Nanocrystals**

By *Yunchao Li*, *Mingfu Ye*, *Chunhe Yang*, *Xiaohong Li*, and *Yongfang Li**

Composition-tunable $Zn_xCd_{1-x}S$ alloyed nanocrystals have been synthesized by a new approach consisting of thermolyzing a mixture of cadmium ethylxanthate ($Cd(exan)_2$) and zinc ethylxanthate ($Zn(exan)_2$) precursors in hot, coordinating solvents at relatively low temperatures (180–210 °C). The composition of the alloyed nanocrystals was accurately adjusted by controlling the molar ratio of $Cd(exan)_2$ to $Zn(exan)_2$ in the mixed reactants. The alloyed $Zn_xCd_{1-x}S$ nanocrystals prepared in HDA/TOP (HDA: hexadecylamine; TOP: trioctylphosphane) solution exhibit composition-dependent shape and phase structures as well as composition-dependent optical properties. The shape of the $Zn_xCd_{1-x}S$ nanocrystals changed from dot to single-armed rod then to multi-armed rod with a decrease of Zn content in the ternary nanoparticles. The alloying nature of the $Zn_xCd_{1-x}S$ nanocrystals was consistently confirmed by the results of high-resolution transmission electron microscopy (HRTEM), X-ray diffraction (XRD), and UV-vis absorption and photoluminescence (PL) spectroscopy. Further, the shape-controlled synthesis of the ternary alloyed nanocrystals was realized by selecting appropriate solvents. Uniform nanodots in the whole composition range were obtained from TOPO/TOP solution, (TOPO: trioctylphosphane oxide) and uniform nanorods in the whole composition range were prepared from HDA/OA solution (OA: octylamine). The effect of the reaction conditions, such as solvent, reaction temperature, and reaction time, on the PL spectra of the alloyed $Zn_xCd_{1-x}S$ nanocrystals was also systematically studied, and the reaction conditions were optimized for improving the PL properties of the nanocrystals.

1. Introduction

Colloidal semiconductor nanocrystals (SNCs) have drawn much attention in recent years due to their unique size-dependent optical and electronic properties,[1] as well as their promising applications in solar cells,[2] light-emitting diodes,[3] biological labeling,[4] and optical sensing,[5] etc. The most important result so far is the synthesis of high-quality SNCs with superior optical properties (such as color-tunable emission, high photoluminescence (PL) quantum yield, high color purity, or narrow emission spectra width and good optical stability, etc.). Thus, in the last decades, much effort has been devoted to the preparation of binary II–VI semiconductor nanocrystals possessing attractive optical properties. Application of the core–shell technique, in particular, has markedly improved the luminescence properties of binary SNCs.[6]

The optical properties (absorption and PL spectra) of binary SNCs can be tuned by changing their particle size. However, tuning the optical properties by changing the particles' size could cause problems (such as the instability of very small nanoparticles) in many applications. In addition, it is difficult to achieve high color purity for binary SNCs because of their size dispersity. Very recently, a method to tune the emission spectra of nanocrystals by changing the constituent stoichiometry in ternary nanocrystals has been reported in the literature.[3c,7–9] Zhong et al.[9] have synthesized $Zn_xCd_{1-x}S$ nanocrystals at high temperature by the reaction of a mixture of CdO and ZnO oleic acid complexes with sulfur in a noncoordinating solvent (octadecene) system. Interestingly, they found that the nanocrystals show narrow and composition-dependent photoluminescence spectra.

Here we report a new approach to synthesize composition-tunable $Zn_xCd_{1-x}S$ alloyed nanocrystals at lower temperature by thermolyzing a mixture of cadmium ethylxanthate ($Cd(exan)_2$) and zinc ethylxanthate ($Zn(exan)_2$) precursors in coordinating solvents. The $Zn_xCd_{1-x}S$ nanocrystals formed exhibit color-tunable (composition-dependent) emission, high color purity, and composition-dependent shape and phase structures. Furthermore, the shape-controlled synthesis of ternary nanocrystals in the whole composition range was realized by selecting appropriate solvents. To the best of our knowledge this is the first report on the shape-controlled synthesis and the observation of a composition-dependent shape transition in ternary alloyed nanocrystals.

[*] Prof. Y. F. Li, Y. C. Li, M. F. Ye, Prof. C. H. Yang, X. H. Li
CAS Key Laboratory of Organic Solids, Center for Molecular Science
Institute of Chemistry, Chinese Academy of Sciences
Beijing 100080 (P.R. China)
E-mail: liyf@iccas.ac.cn, Fax: 86-10-62559373
Y. C. Li, X. H. Li
Graduate School, Chinese Academy of Sciences
Beijing 100039 (P.R. China)

[**] This work was supported by the State Key Basic Research Project (No. 2001CB610507, 2002CB613401), and an "863" project from the Ministry of Science and Technology of China.

DOI: 10.1002/adfm.200400320

2. Results and Discussion

2.1. Characterization of Ternary $Zn_xCd_{1-x}S$ Alloyed Nanocrystals Prepared in HDA/TOP Solution

The $Zn_xCd_{1-x}S$ ternary alloyed nanocrystals were prepared by thermolyzing a hot HDA/TOP (HDA: hexadecylamine; TOP: trioctylphosphane) solvent mixture of the $Cd(exan)_2$ and $Zn(exan)_2$) precursors at 210 °C for 3 h. For comparison, binary ZnS and CdS nanocrystals were also prepared by a similar route (see Experimental sect.). The composition of the alloyed nanocrystals was adjusted by changing the molar ratio of $Zn(exan)_2$ to $Cd(exan)_2$ (see Table 1). In the preparation of ternary alloyed nanocrystals reported in the literature, the Zn/Cd ratio in the reactants is obviously higher than that found here[9–13] because the reaction of Cd with S is faster than that of Zn with S in those reaction systems. In our case, very interestingly, the Zn/Cd ratio in the formed $Zn_xCd_{1-x}S$ nanocrystals is almost identical to that in the reactant mixtures over a large composition range (from $x = 0.13$ to $x = 0.78$), as shown in Table 1. This consistency could be a result of the similar reaction activity and good co-dissolving property of the two precursors used in the current method. The fact that the Zn/Cd ratio in the formed nanocrystals agrees with that in the reaction mixture makes composition adjustment of the alloyed nanocrystals easier and more accurate. More importantly, these composition-tunable $Zn_xCd_{1-x}S$ nanocrystals exhibit special composition-dependent properties, which will be discussed in the following sections.

Table 1. Composition (Zn/Cd molar ratio) of the reactant solutions and the formed $Zn_xCd_{1-x}S$ nanocrystals

Samples	TZCS-1	TZCS-2	TZCS-3	TZCS-4	TZCS-5	TZCS-6
Molar ratio of Zn/Cd ($Zn(exan)_2$/ $Cd(exan)_2$)	1:6 (0.17)	1:4 (0.25)	1:2 (0.50)	1:1 (1.0)	2:1 (2.0)	4:1 (4.0)
Molar ratio of Zn/Cd in the alloyed nanocrystals, as determined by ICP	0.15	0.28	0.48	0.96	1.89	3.60
x	0.13	0.22	0.32	0.49	0.65	0.78

2.1.1. Shape Variation of $Zn_xCd_{1-x}S$ Nanocrystals with the Change of Composition

Figure 1 shows transmission electron microscopy (TEM) images of ZnS, $Zn_xCd_{1-x}S$ (from TZCS-1 to TZCS-6, formed with different compositions, see Table 1), and CdS nanocrystals. The preparation of the nanocrystals is described briefly in the above paragraph and in the Experimental section. The ZnS nanocrystals are mainly monodisperse spherical particles (dots), with an average diameter of 5.0 nm, and are self-assembled into an ordered array, while the CdS nanocrystals are uniform, multi-armed rods with an average length of 22 nm and width of 4.0 nm. For the $Zn_xCd_{1-x}S$ nanocrystals, very interestingly, a shape transition from dot to single-armed rod then to multi-armed rod occurs with a decrease of Zn content in the particles. When x (Zn content) equals 0.78, hexagonally assembled, uniform spherical particles (very similar to the case of ZnS) with an average size of 6.0 nm in diameter were formed. As x was decreased to 0.65, some elongated or oblong particles were formed together with the spherical particles, and as x was decreased further to 0.49, single-armed and bent short rods became dominant. When x was further decreased to 0.22 and 0.13, the formed particles in both cases showed a multi-armed rod shape (very similar to the case of CdS) with average sizes of 18 nm in length and 4.4 nm in width for $x = 0.22$, and 14 nm in length and 4.6 nm in width for $x = 0.13$. The inserted high-resolution TEM (HRTEM) images in Figures 1b–f show well-resolved lattice fringes, demonstrating the highly crystalline nature of the formed $Zn_xCd_{1-x}S$ nanocrystals, and revealing the gradual increase of the interplanar distances of the {002} plane (from 0.32 nm for TZCS-4 ($x = 0.49$) to 0.33 nm for TZCS-3 ($x = 0.32$) then to 0.36 nm for TZCS-2 ($x = 0.22$).These results mean that the c axes of the $Zn_xCd_{1-x}S$ nanocrystals extend with an increase of Cd content, which is evidence for the formation of ternary alloyed nanoparticles.

The reason for the composition-induced shape transition could be as follows: the energy difference between wurtzite and zincblende structures in CdS is smaller than that in ZnS,[14,15] and wurtzite CdS is more stable than wurtzite ZnS.[16–18] Therefore, for CdS, it is easy to produce a zincblende "core" at the nucleation stage but form a wurtzite arm in the following growth process under kinetic control.[19] As a result, multi-armed CdS nanorods are formed. For the ZnS nanocrystals, however, the zincblende structure always dominates the growth processes of the nanocrystals, with only a few wurtzite-type stacking faults being present (see the X-ray diffraction (XRD) patterns in Fig. 2). Because of the high symmetry of the zincblende structure, only dot-shaped ZnS nanocrystals are obtained. As for the growth of the $Zn_xCd_{1-x}S$ ternary nanocrystals, the two reactants—$Zn(exan)_2$ and $Cd(exan)_2$—were dissolved in the solvent and are therefore mixed on a molecular level with each other. Accordingly, a solid solution of $Zn_xCd_{1-x}S$ nanocrystals would be formed during the thermolysis processes, and the growth of the nanocrystals would involve competition between the ZnS-like (dot) and the CdS-like (multi-armed rod) growth modes. Therefore, the Zn/Cd molar ratio in the reactants mixture influences the growth process and results in the different shapes of the formed $Zn_xCd_{1-x}S$ nanocrystals. Moreover, a small Cd content seems to have a more striking impact than a small Zn content on the shape of the formed $Zn_xCd_{1-x}S$ nanocrystals, since the shape of some $Zn_xCd_{1-x}S$ nanocrystals at $x = 0.65$ already deviates from that of a dot. When the Zn/Cd molar ratio in the mixture is close to 1 (e.g., $x = 0.49$), the resulting particles have a single-armed or bent-rod shape because of the limitation of monomer concentration.

ADVANCED FUNCTIONAL MATERIALS

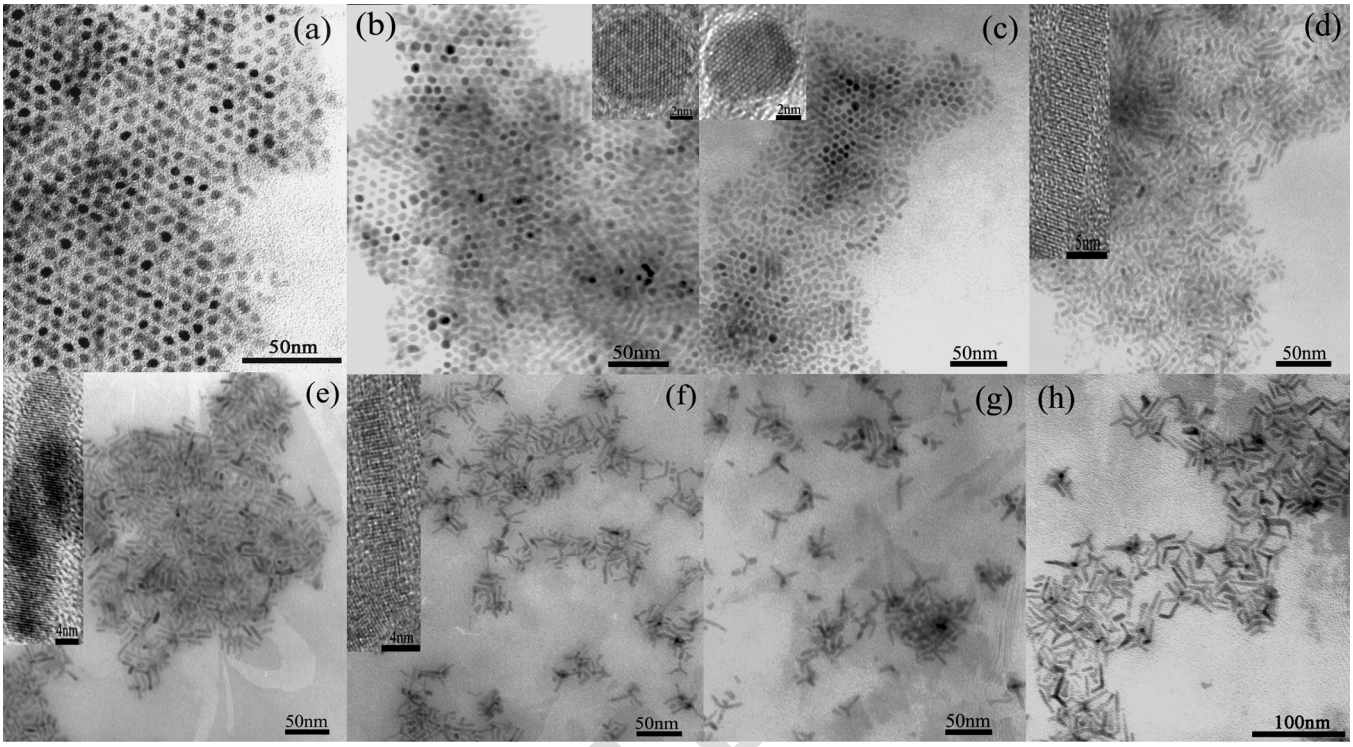

Figure 1. TEM images of ZnS (a), $Zn_xCd_{1-x}S$ ($x = 0.78$ (b), 0.65(c), 0.49(d), 0.32(e), 0.22(f), 0.13(g)), and CdS nanocrystals (h) synthesized in HDA/TOP solution. The inserts in (b–f) are the corresponding HRTEM images.

2.1.2. Phase-Structure Transition of $Zn_xCd_{1-x}S$ Nanocrystals with a Change of Composition

Figure 2 shows the powder XRD patterns of ZnS, CdS, and the alloyed $Zn_xCd_{1-x}S$ nanocrystals. All XRD patterns show obvious size-broadening effects, indicating the finite size of these nanocrystals. For CdS, the XRD pattern can be indexed as a wurtzite-phase structure with strongly characteristic (100), (002), (101), (102), (110), (103), and (112) peaks, while for ZnS the XRD pattern mainly reflects its zincblende character (strong (111), (220), and (311) peaks) with some weak wurtzite character (such as the existence of a vague (103) and a deformed (111) peak), which indicates either that the ZnS particles have a zincblende structure with some wurtzite defaults or that most particles have a zincblende structure with others having a wurtzite structure. As for the $Zn_xCd_{1-x}S$ nanocrystals the diffraction peaks in the XRD patterns gradually shift to larger angles and a phase transition from wurtzite to zincblende occurs with an increase of Zn content. This continuous peak shifting of the nanocrystals also indicates that there is no phase separation or separated nucleation of ZnS or CdS in the $Zn_xCd_{1-x}S$ nanocrystals. As shown in Figure 3, in the composition region of x between 0.1 and 0.6, a linear compression in both the a and c axes of the $Zn_xCd_{1-x}S$ nanocrystals is observed, consistent with Vegard's law.[8,9,20] The deviation of the values of the a axes and c axes from linearity at high Zn content ($x > 0.6$) can be attributed to a phase-structure change in this region.

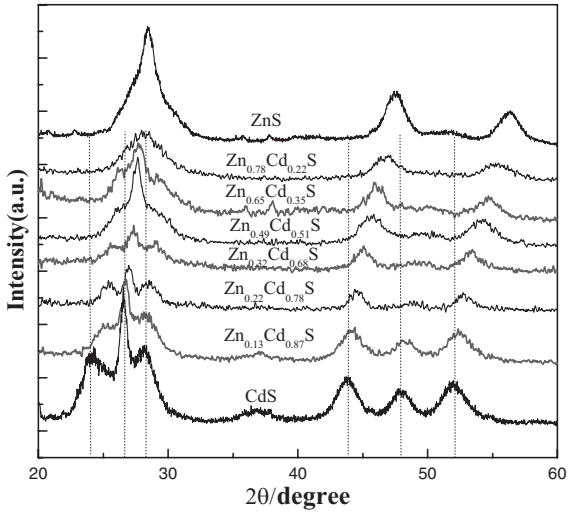

Figure 2. Powder XRD patterns of ZnS, $Zn_xCd_{1-x}S$ (TZCS-1–6) and CdS nanocrystals.

2.1.3. Composition-Dependent Optical Properties

Figure 4 shows the absorption spectra of ZnS, CdS, and $Zn_xCd_{1-x}S$ nanocrystals. For ZnS and CdS, the absorption edges are located at about 325 nm and 492 nm, respectively. The absorption edges of the samples were determined by extrapolation after performing a linear regression on the absorption-edge data. As for the $Zn_xCd_{1-x}S$ nanocrystals, their

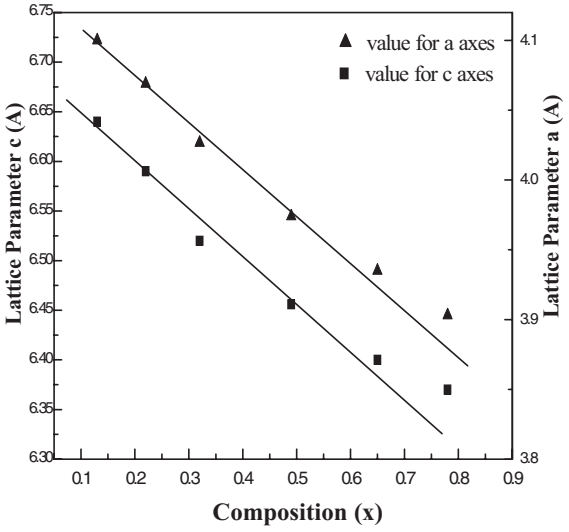

Figure 3. The *a* (▲) and *c* (■)-axis values of the $Zn_xCd_{1-x}S$ nanocrystals as a function of Zn content (*x*).

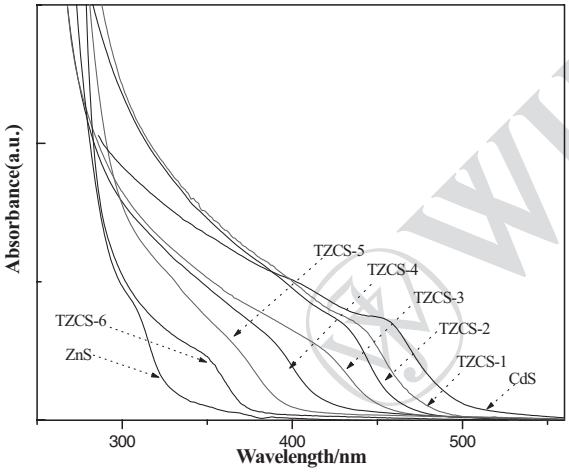

Figure 4. UV-vis absorption spectra of ZnS, $Zn_xCd_{1-x}S$ (TZCS-1–6), and CdS nanocrystals.

absorption edges gradually shift from 372 nm to 470 nm as the Zn content (*x* value) in the particles decreases from 0.78 to 0.13. Obviously, such a large shift in the absorption edge cannot be attributed to quantum-size effects, but could be due to a continuous shift of the energy bandgap (E_g) of the nanoparticles with a change in their composition.[9–13,21] We calculated the bandgap values ($E_{g(x)}$) of the $Zn_xCd_{1-x}S$ nanocrystals from the absorption edges. Figure 5 shows the bandgap energy as a function of the Zn content (*x*) for the $Zn_xCd_{1-x}S$ nanocrystals. The results in Figure 5 can be well fitted by the empirical relationship[12,13] for bulk $Zn_xCd_{1-x}S$: $E_{g(x)} = 2.5 + 0.59x + 0.61x^2$; the quantum-size confinement effect is not obvious.

The $Zn_xCd_{1-x}S$ nanocrystals are actually in the weak quantum-confinement regime because their particle radii are close to, or somewhat larger than, the corresponding Bohr exciton radius (the average radius of samples TZCS-1 to TZCS-6 is 2.3,

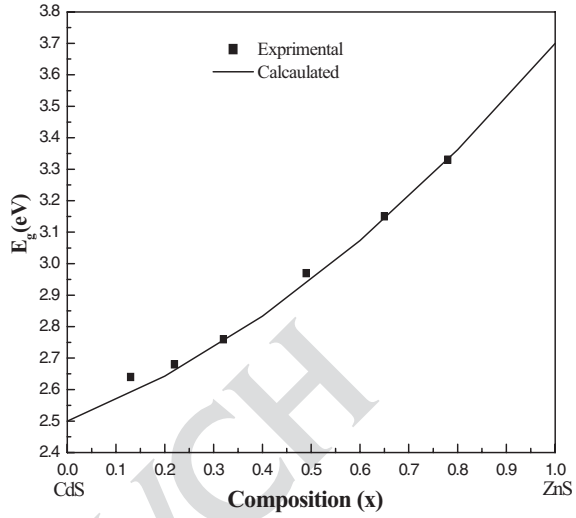

Figure 5. Bandgap energy as a function of the alloy Zn composition (*x*) for the $Zn_xCd_{1-x}S$ nanocrystals (square, this work) and bulk $Zn_xCd_{1-x}S$ (line, calculated from the empirical relation).

2.2, 2.4, 2.4, 2.8, and 3.0 nm, respectively (see Fig. 1), while the corresponding Bohr exciton radius is 2.9, 2.8, 2.7, 2.6, 2.5, and 2.4 nm, respectively[9]). Regardless of the shape effect, the quantum-size effect in semiconductor solid solutions can be calculated quantitatively based on the effective mass model using the formula[1a,12a,22]

$$E_{n(R,x)} = E_{g(x)} + \frac{\pi^2\hbar^2}{2R^2}\left[\frac{1}{m_e^*(x)} + \frac{1}{m_h^*(x)}\right] - \frac{1.786e^2}{\varepsilon R} - \frac{0.124e^4}{\hbar^2\varepsilon^2}\left[\frac{1}{m_e^*(x)} + \frac{1}{m_h^*(x)}\right] \quad (1)$$

where $E_{g(x)}$, R, $m_e^*{}_{(x)}$, $m_h^*{}_{(x)}$, and ε are the bandgap energy for a bulk solid solution (at composition *x*), the radius of the particle, the effective masses of electron and hole in the particles with composition *x*, and the dielectric constant, respectively. To perform such a calculation we assumed that $m_e^*{}_{(x)}$, and $m_h^*{}_{(x)}$ are linearly dependent on the composition *x*, and used the values $E_g = 3.7$ eV, $\varepsilon = 5.4$, $m_e^* = 0.42$, and $m_h^* = 0.61$ for ZnS, and $E_g = 2.5$ eV, $\varepsilon = 5.3$, $m_e^* = 0.18$, and $m_h^* = 0.53$ for CdS.[12,13] The results indicate that when $x = 0.65$ the energy difference between the particles with radii of 3.0 and 2.5 nm is very small (0.086 eV), that is, the quantum-size effect in the nanoparticles with this relatively large size is very weak. Thus, the absorption edge (and the emission-peak position discussed in the next paragraph) of the nanocrystals depends mainly on their composition.

Figure 6 shows the corresponding PL spectra of the nanocrystals. The PL spectra of ZnS and CdS nanocrystals display similar characteristics: two emission peaks—a bandgap and a trapped emission—can be observed. The bandgap emission is sharp and located near the absorption edge of the particle, while the trapped emission is broad and Stokes-shifted to longer wavelengths, while for the $Zn_xCd_{1-x}S$ nanocrystals only a

ADVANCED FUNCTIONAL MATERIALS

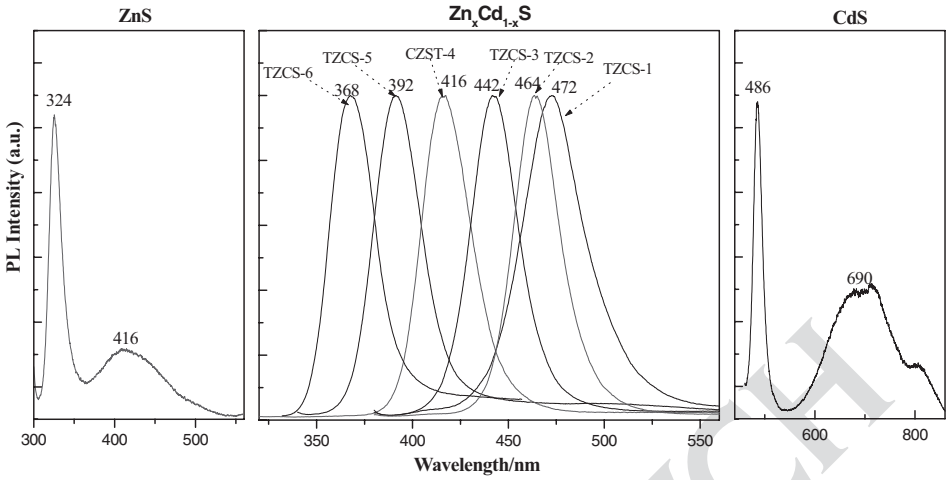

Figure 6. PL spectra of ZnS, $Zn_xCd_{1-x}S$ (TZCS-1–6), and CdS nanocrystals.

symmetric and narrow bandgap-emission peak (25 nm at its average full width at half maximum (fwhm)) appears in the PL spectrum and this peak shifts systematically from 368 to 472 nm as the composition x decreases from 0.78 to 0.13. This sole emission peak in the PL spectrum indicates that surface-defect emission is suppressed and that alloyed $Zn_xCd_{1-x}S$ nanocrystals have indeed formed. In fact, the continuous and significant shift of the bandedge emission peaks and the absorption edges of the resulting ternary nanocrystals with composition (x) is the most direct evidence for the formation of alloyed $Zn_xCd_{1-x}S$ nanocrystals rather than separate ZnS, CdS, or core–shell-structured nanocrystals.[9–13,21] In dilute solution, if ZnS or CdS nucleate separately, their corresponding PL and absorption peaks should appear. The unique PL and absorption peak of the resulting $Zn_xCd_{1-x}S$ nanocrystals rules out this separate nucleation, which is in agreement with the results of the HRTEM and XRD measurements. If a core–shell structure is formed, such a significant shift of the optical spectra cannot be produced relative to those of the core materials.

The relatively narrow PL peak (25 nm at its average fwhm) of the $Zn_xCd_{1-x}S$ nanocrystals is mainly due to the relatively homogeneous size distribution (size fluctuation is less than 10 %), which is a result of the good size control in the experiment and the effective suppression of inhomogeneous spectral broadening by the formation of an alloy structure. As mentioned above, the resulting $Zn_xCd_{1-x}S$ nanocrystals are in the weak quantum-confinement regime—their bandgap energy becomes insensitive to the size in the sample size range. However, if the size difference of the nanoparticles is prominent (such as, it exceeds 2.0 nm), the PL peak would be broadened obviously.

The PL quantum yields (PLQYs) of the $Zn_xCd_{1-x}S$ nanocrystals at room temperature are about 5–8 %, lower than the best values reported previously by Zhong et al.[9] These lower PLQYs may be due to the existence of some surface disorder and surface degradation of the nanocrystals due to a nonequilibrium growth environment—the release of some quantities of gas at the nucleation stage, the fast reaction rate in the subsequent growth process,[23] and an unsuitable annealing temperature—of the nanocrystals. However, considering that the emission of nanocrystals in the blue range is usually weak (< 5 %), our value is acceptable and could be further enhanced by optimization of the reaction conditions. In summary, the $Zn_xCd_{1-x}S$ nanocrystals prepared in this work exhibit promising optical properties: color-tunable emission, high color purity, and moderate PLQYs.

2.2. Shape-Controlled Synthesis of Alloyed Nanocrystals and Their Optical Properties

The shape-controlled synthesis of SNCs and the investigation of their shape-related optical properties are important issues in nanoscience, and have attracted significant attention recently. However, there are few reports related to these two issues with alloyed ternary nanocrystals. As for the shape-controlled synthesis, because different components in the ternary system usually have different activities and different growth modes, the shape of the resulting particles should exhibit some composition dependency, as mentioned in the previous sections of this paper. So, it is difficult to exert shape control over the whole composition range (except for the cases of the formation of nanodots in the thermodynamic control regime[9] and the formation of zincblende nanodots in an aqueous solution[12]).

In this work we have synthesized uniform nanorods or nanodots over the whole composition range by changing the coordinating solvent. As mentioned above (see Fig. 1), in an HDA/TOP solution the shape of the resulting $Zn_xCd_{1-x}S$ nanocrystals is composition-dependent: uniform, alloyed multi-armed nanorods are attained in the high Cd-content range (e.g., $x = 0.22$ or 0.13), while uniform, alloyed nanodots are formed in the high Zn-content range (e.g., $x = 0.78$). Interestingly, when we used TOPO/TOP (TOPO: trioctylphosphane oxide) instead of HDA/TOP as the solvent, uniform nanodots of $Zn_xCd_{1-x}S$ alloyed nanocrystals were obtained even in the high Cd-content range (e.g., $x = 0.22$), as shown in Figure 7a, while in an HDA/

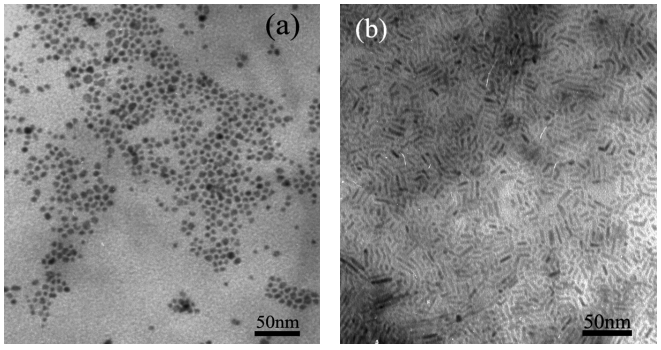

Figure 7. TEM imagies of $Zn_xCd_{1-x}S$ alloyed nanocrystals synthesized in a) TOPO/TOP solution with $x = 0.22$, and b) HDA/OA solution with $x = 0.78$.

OA solution (OA: octylamine) uniform nanorods of $Zn_xCd_{1-x}S$ nanocrystals were synthesized even in the high Zn-content range (e.g., as $x = 0.78$; see Fig. 7b). In this way, we have realized the shape-controlled synthesis of $Zn_xCd_{1-x}S$ nanocrystals by selecting the appropriate solvents. For example, to synthesize uniform nanodots over the whole composition range we can utilize TOPO/TOP solution (or use HDA/TOP in the case of high Zn content); to prepare uniform nanorods in the whole composition range, we can use an HDA/OA solution (or use HDA/TOP in the case of high Cd content).

The effect of the ligand molecules on the shape of the resulting alloyed ternary nanocrystals could come from the difference in their coordinating ability and steric conformation.[18b,23,24] For example, in the preparation of the binary ZnS and CdS nanocrystals, nanodots were obtained in TOPO/TOP solution[18b,24a,25] while nanorods were formed in HDA/OA (or in HDA or HDA/TOP) solution,[18b,24b] even though a similar synthetic route and reaction conditions were utilized in both cases.

Figure 8 compares the UV-vis absorption and PL spectra of the nanodots and nanorods of the alloyed $Zn_xCd_{1-x}S$ nanocrystals with high Cd content and high Zn content. For the $Zn_xCd_{1-x}S$ nanocrystals with high Cd content (e.g., $x = 0.22$), where the nanodots were obtained from TOPO/TOP solution and the nanorods were prepared from HDA/TOP solution, the UV-vis absorption spectrum of the nanodots is similar to that of the nanorods; however, the PL spectrum of the nanodots shows obvious differences compared to that of the nanorods (see Fig. 8a): here are two PL emission peaks at 466 nm and 650 nm, respectively, for the nanodots, while there is only one PL peak at 464 nm for the nanorods. The broad PL peak at longer wavelength (650 nm) for the nanodots should come from a trapped emission that may be due to imperfect surface passivation by TOPO molecules. The bandgap emission-peak position of the nanodots is close to that of the nanorods, which may be attributed to the relatively large and similar diameters of the rods (4.4 nm) and the dots (4.8 nm). In the weak quantum-confinement regime, the emission-peak positions depend more sensitively on diameter than on length at a small aspect ratio.[26] For those $Zn_xCd_{1-x}S$ nanocrystals with high Zn content (e.g., $x = 0.78$), where the nanodots were obtained from HDA/TOP solution and the nanorods were prepared from HDA/OA solution, the absorption edge and PL emission peak of the nanorods show a blue-shift with respect to those of the nanodots (see Fig. 8b). Since the composition of the nanocrystals is the same, the blue-shift of the absorption and PL spectra should be due to the quantum-size effect. Moreover, compared to the nanodots, the PL emission peak of the nanorods shows some asymmetry, which may be resulted from the incomplete anneal of the nanorods formed under relatively low temperature. These results also suggest that the surface states of the alloyed nanoparticles also have an important effect on their PL properties.

2.3. The Influence of Reaction Conditions on the Optical Properties of the $Zn_xCd_{1-x}S$ Alloyed Nanocrystals

For binary SNCs, it is well known that the PL properties of the nanoparticles are strongly dependent on their surface

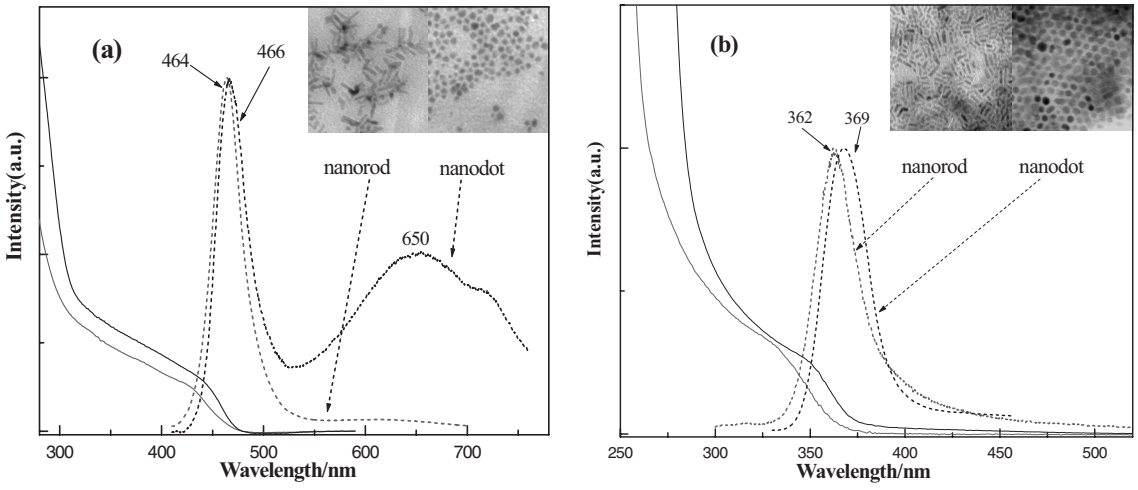

Figure 8. UV-vis absorption and PL spectra for the nanodots and nanorods of the $Zn_xCd_{1-x}S$ nanocrystals with different compositions of a) high Cd content ($x = 0.22$), and b) high Zn content ($x = 0.78$).

states, surface passivation, and size distribution.[27–30] To achieve good PL properties, a moderately stable and equilibrated growth environment must be attained[28–30]—at is to say that the PL properties of the SNCs are reaction-condition- and process-dependent. As far as the alloyed ternary SNCs are concerned, the above situation also applies, and, moreover, the component uniformity also plays a key role. Because the factors mentioned above are mostly related to the reaction conditions (such as ligand, reaction temperature, and reaction time), we systematically investigated the effect of those reaction conditions on the PL spectra of the alloyed nanocrystals in order to further improve their PL properties. The results are shown in Figure 9. It can be seen from Figure 9a that the ligand has an important impact on the PL spectra of the resulting nanocrystals. Obviously, the particles formed in linear alkylamine (HDA, OA) solutions exhibit better PL properties (stronger PL intensity and narrower fwhm) than those formed in TOPO or trioctylamine (TOA) solutions as the linear alkylamine molecules can passivate the surface and control the interaction between the nanocrystals and their environment better.[27,28] Therefore, to attain good PL properties a linear alkylamine is a better ligand than those with large steric barriers for the preparation of $Zn_xCd_{1-x}S$ alloyed nanocrystals.

The reaction temperature also has a direct influence on the intensity and the symmetry of the PL peaks (see Fig. 9b). As the temperature increases, the PL peak exhibits a moderate red-shift and becomes weaker but more symmetric, while the trapped emission (around 600 nm) gradually loses its intensity.

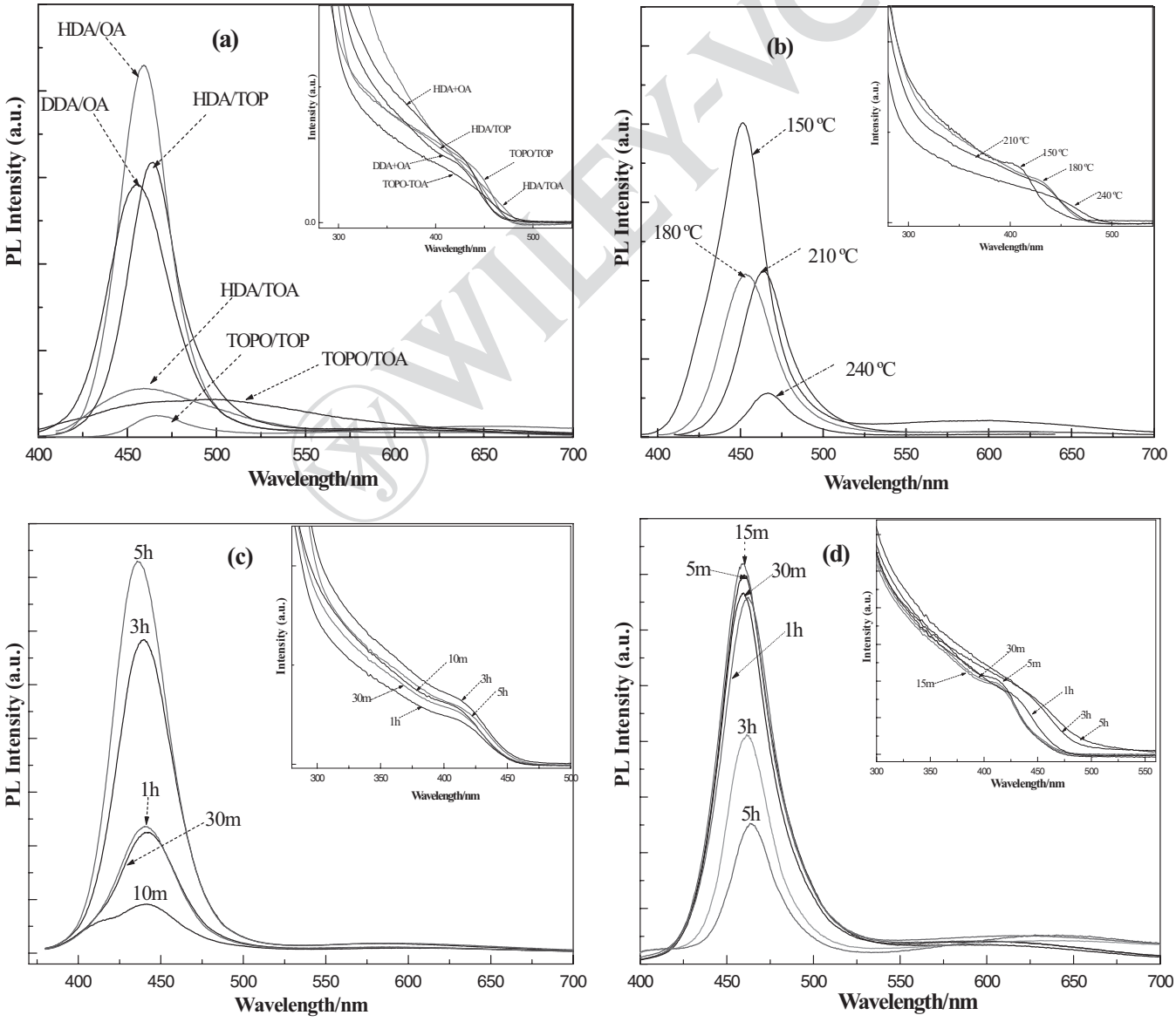

Figure 9. PL spectra of $Zn_xCd_{1-x}S$ alloyed nanocrystals with $x = 0.22$ synthesized with the same precursor composition (Cd/Zn = 4) but under different conditions: a) in different ligand solutions, at 210 °C, and reaction for 3 h; b) at different reaction temperature (150 °C, 180 °C, 210 °C, 240 °C), in HDA/TOP solution, and reaction for 3 h; c) in HDA/OA solution, at 210 °C, and reaction for different times (10 min, 30 min, 1 h, 3 h, 5 h); and d) in HDA/TOP solution, at 210 °C, and reaction for different times (5 min, 15 min, 30 min, 1 h, 3 h, 5 h). The insets in the figures are the corresponding absorption spectra.

This phenomenon indicates that a higher temperature (higher thermal drive) favors the reduction of the deep trap (or defect) in the nanocrystals[28,29] and promotes the migration of different atoms in the matrix of the nanocrystals to form a homogenous solid solution during the annealing process. However, as mentioned above, a perfect surface state is the result of close-to-equilibrium growth under adequate thermodynamic and kinetic control—a too-high or too-low reaction drive (reaction temperature) usually results in surface defects, disorder, or phase separation. In addition, a fast growth rate and high reaction temperature usually easily results in size dispersity at high reaction temperature usually results in size dispersity. Thus, there is an optimal temperature range (180–210 °C) for the growth of high-quality alloyed nanocrystals.

The effect of reaction time on the PL spectra also depends on the nature of the ligand solvents. With a longer reaction time the PL peak becomes stronger and more symmetric in the HDA/OA solution system (Fig. 9c), while it becomes weaker and the trapped emission at longer wavelength becomes relatively stronger in the HDA/TOP solution system (Fig. 9d). Why does the reaction time affect the PL intensity of the nanocrystals so dramatically, and what is the reason for the different influence of the reaction time in different ligand solutions? As mentioned above, the PL properties of the SNCs are reaction-condition- and process-dependent. The most-favorable surface structure of nanocrystals in a solution with a defined amount of monomer is probably only stable for a short period of time due to the rapid variation of the monomer concentration,[29] and the formation of a homogenous solid solution is a time-consuming process, therefore there is an optimal reaction time (1–3 h for the HDA/OA system or 30 min to 1 h for the HDA/TOP system) during which the nanocrystals can achieve optimal surface structure, good crystallinity, and uniform composition, and still exhibit a maximum of the bandedge emission. The different influence of the reaction time in different ligand solutions may be due to the lower reaction temperature during the initial stage in HDA/OA solution (due to the reflux behavior of OA) than in HDA/TOP solution and the weaker passivation ability of TOP than HDA for the nanocrystals.

Based on the above results, for the alloyed $Zn_xCd_{1-x}S$ nanocrystals, the maximum PLQY and the narrowest fwhm are about 16 % and 22 nm, respectively, under the optimal reaction conditions (180–200 °C and reaction for 2–4 h in HDA/OA solution).■1–3 hours above■

3. Conclusion

We have reported a new approach to synthesize $Zn_xCd_{1-x}S$ alloyed nanocrystals at relatively lower temperatures. They were prepared by thermolyzing a mixture of cadmium ethylxanthate and zinc ethylxanthate precursors in a hot coordinating solvent. Composition adjustment of the $Zn_xCd_{1-x}S$ nanocrystals was achieved by changing the molar ratio of $Cd(exan)_2$ to $Zn(exan)_2$ in the mixture. The Zn/Cd molar ratio in the formed nanocrystals is almost the same as that in the reactant mixture over a large composition region, which makes composition adjustment of the $Zn_xCd_{1-x}S$ alloyed nanocrystals easy and accurate. The formed alloyed $Zn_xCd_{1-x}S$ nanocrystals exhibit a special composition-inducing shape change (from nanodot to bent nanorod, then to multi-armed nanorod) and phase-structure transition (from wurtzite to zincblende) with a decrease of x, and show good optical properties (emission-tunable (PL emission peaks shift from 368 to 472 nm, and high color purity (25 nm at the fwhm)). The alloy nature of the $Zn_xCd_{1-x}S$ nanocrystals was also consistently confirmed by the results of HRTEM and XRD, and UV-vis absorption and PL spectroscopy. Furthermore, the shape-controlled synthesis and shape-related optical properties in the ternary alloyed nanocrystals system were investigated. The shape of the alloyed particles could be controlled from uniform dot to uniform rod over the full composition range by the selection of an appropriate coordinating solvent. To the best of our knowledge, this is the first report of the shape-controlled synthesis and a composition-induced shape transition in ternary alloyed nanocrystal systems. Moreover, the influence of ligands, reaction temperature, and reaction time on the PL properties of the alloyed $Zn_xCd_{1-x}S$ nanocrystals was also systematically studied. Based on this investigation we greatly improved the PL properties of the ternary nanocrystals: the maximum PLQY and the narrowest fwhm are about 16 % and 22 nm, respectively, under the optimal reaction conditions. In summary, these alloyed $Zn_xCd_{1-x}S$ nanocrystals exhibit good optical properties and are promising candidates for use as emitting materials in nanodevices or for biological labeling.

4. Experimental

Materials: Zinc acetate, cadmium chloride, potassium ethylxanthate, methanol, chloroform, and toluene (Beijing Chemical Reagent Ltd. Co. of China) were analytical grade reagents. Trioctylphosphane oxide (TOPO, 90 %, Aldrich), Trioctylphosphane (TOP, 90 %, Alfa), hexadecylamine (HDA, 90 %, Aldrich), dodecylamine (DDA, 98 %, Acros), octylamine (OA, 98 %, Aldrich), and trioctylamine (TOA, 98 %, Acros) were used as received without further purification. Zinc ethylxanthate ($Zn(exan)_2$) and cadmium ethylxanthate ($Cd(exan)_2$) were synthesized by a method similar to that use by Nair et al. [25].

Synthesis and Purification: Typically, all the synthetic processes were carried out under an inert atmosphere. The $Zn_xCd_{1-x}S$ alloyed nanocrystals were prepared as follows (Protocol A): $Zn(exan)_2$ and $Cd(exan)_2$ with a specified molar ratio (from 1:6 to 4:1) and a total molar amount of 0.6 mmol were mixed together and dissolved in 3 mL of TOP (or OA), then the solution was swiftly injected into 6.0 g of hot HDA (or DDA or TOPO) solution with a syringe under stirring, and the reaction temperature was maintained at 210 °C for 3 h. The resulting colloidal samples were labeled as TZCS-1 to TZCS-6 for the molar ratios of $Zn(exan)_2$ to $Cd(exan)_2$ 1:6, 1:4, 1:2, 1:1, 2:1, and 4:1, respectively. ZnS and CdS nanocrystals were synthesized as follows (Protocol B) [18b,24]: A specified amount of $Zn(exan)_2$ or $Cd(exan)_2$ was dissolved in a 3 mL of TOP, and then the solution was swiftly injected into 6.0 g of hot HDA solution, with the other reaction conditions being similar to Protocol A. Afterwards, the colloid solutions obtained in Protocols A and B were cooled, and precipitated by addition of acetone (or methanol). The flocculent precipitate formed was centrifuged and the upper liquid was decanted. The isolated solid was then dispersed in chloroform (or toluene). The above centrifugation and isolation procedure was repeated several times to purify the nanocrystals.

ADVANCED FUNCTIONAL MATERIALS

Finally, the purified nanocrystals were re-dispersed in chloroform (or toluene) for the preparation of transmission electron microscopy (TEM) specimens, or dried under vacuum for XRD and inductively coupled plasma (ICP) measurements.

Characterization: For the measurement of the absorption and photoluminescence (PL) spectra of the nanocrystals, needle-tip aliquots were taken from the reaction flask at given time intervals and dissolved in about 2 mL of chloroform. The sample solutions were put in a 1 cm quartz cell; chloroform was used as the reference solution. UV-vis absorption spectra were recorded on a Hitachi U-3010 spectrophotometer. PL spectra were measured on a Hitachi F-4500 spectrophotometer. The slits were set to 2.5 nm. The room-temperature PL quantum yield (PLQY) was determined by comparing the integrated emission of the samples in chloroform with that of a fluorescent dye (9,10-diphenylanthracene). To avoid obvious re-absorption, low concentration solutions were used—the optical densities of all the samples were adjusted to below 0.1 at the excitation wavelengths (which were set slightly to the blue side of the first absorption peak of the samples). TEM observations were performed with a Hitachi H-800 transmission electron microscope, accompanied by selected-area electron diffraction (SAED). High-resolution transmission electron microscopy (HRTEM) measurements were carried out using a Hitachi H-9000NAR transmission electron microscope operating at 200 kV. The specimens for the TEM measurements were prepared by depositing a drop of a dilute toluene solution of the samples on a carbon-coated copper grid and drying at room temperature. X-ray diffraction (XRD) patterns were recorded with a Rigaku D/max-2400 diffractometer operating at 40 kV and 120 mA with Cu $K\alpha$ radiation. Samples for XRD measurements were solid powders prepared by drying the purified product under vacuum. The compositions of the alloyed nanocrystals were measured by means of inductively coupled plasma atomic emission (ICP) using a standard HCl/HNO_3 digestion.

Received: July 12, 2004
Final version: August 30, 2004

[1] a) M. G. Bawendi, M. L. Steigerwald, L. E. Brus, *Annu. Rev. Phys. Chem.* **1990**, *41*, 477. b) H. Weller, *Angew. Chem. Int. Ed. Engl.* **1993**, *32*, 41. c) C. B. Murray, C. R. Kagan, *Annu. Rev. Mater. Sci.* **2000**, *30*, 545.

[2] a) W. Huynh, J. J. Dittmer, A. P. Alivisatos, *Science* **2002**, *295*, 225. b) B. Q. Sun, E. Marx, N. C. Greenham, *Nano. Lett.* **2003**, *3*, 961.

[3] a) V. L. Colvin, M. C. Schlamp, A. P. Alivisatos, *Nature* **1994**, *380*, 354. b) S. Coe, W. K. Woo, M. Bawendi, V. Bulovic, *Nature* **2002**, *420*, 800. c) E. J. Jang, S, Jun, L. S. Pu, *Chem. Commun.* **2003**, 2964.

[4] a) M. Bruchez, M. Moronne, P. Gin, S. Weiss, A. P. Alivisatos, *Science* **1998**, *281*, 2013. b) W. C. Chan, S. M. Nie, *Science* **1998**, *281*, 2016.

[5] a) C. J. Murphy, *Anal. Chem.* **2002**, *74*, 520A. b) Y. K. Jaiswal, H. Mattoussi, J. M. Mauro, S. M. Simon, *Nat. Biotechnol.* **2003**, *21*, 47.

[6] a) M. A. Hines, P. Guyot-Sionnest, *J. Phys. Chem.* **1996**, *100*, 468. b) B. O. Dabbousi, J. Rodriguez-Viejo, F. V. Mikulec, J. R. Heine, H. Mattoussi, R. Ober, K. F. Jensen, M. G. Bawendi, *J. Phys. Chem. B* **1997**, *101*, 9463. c) X. G. Peng, M. C. Schlamp, A. V. Kadavanich, A. P. Alivisatos, *J. Am. Chem. Soc.* **1997**, *119*, 7019.

[7] R. E. Bailey, S. M. Nie, *J. Am. Chem. Soc.* **2003**, *125*, 7100.

[8] X. H. Zhong, M. Y. Han, Z. L. Dong, T. J. White, W. Knoll, *J. Am. Chem. Soc.* **2003**, *125*, 8589.

[9] X. H. Zhong, Y. Y. Feng, W. Knoll, M. Y. Han, *J. Am. Chem. Soc.* **2003**, *125*, 13 559.

[10] H. C. Youn, S. Baral, J. H. Fendler, *J. Phys. Chem. B* **1988**, *92*, 6320.

[11] L. M. Qi, J. M. Ma, H. M. Cheng, Z. G. Zhao, *Colloids Surf. A* **1996**, *111*, 195.

[12] a) J. Cizeron, M. P. Pileni, *J. Phys. Chem.* **1995**, *99*, 17 410. b) J. Cizeron, M. P. Pileni, *J. Phys. Chem. B* **1997**, *101*, 8887.

[13] D. V. Petrov, B. S. Santos, G. A. L. Pereira, C. de M. Donegaá, *J. Phys. Chem. B* **2002**, *106*, 5325.

[14] C. Y. Yeh, Z. W. Lu, S. Froyen, A. Zunger, *Phys. Rev. B* **1992**, *46*, 10 086.

[15] T. Ito, *J. Appl. Phys.* **1998**, *37*, L1217.

[16] X. J. Chen, H. F. Xu, N. S. Xu, F. H. Zhao, W. J. Lin, G. Lin, Y. L. Fu, Z. L. Huang, H. Z. Wang, M. M. Wu, *Inorg. Chem.* **2003**, *42*, 3100.

[17] K. Murakoshi, H. Hosokawa, N. Tanaka, M. S. Y. Wada, T. Sakata, H. Mori, S. Yanagida, *Chem. Commun.* **1998**, 321.

[18] a) W. L. Wang, F. L. Bai, *ChemPhysChem* **2003**, *4*, 761. b) Y. C. Li, X. H. Li, C. H. Yang, Y. F. Li, *J. Phys. Chem. B* **2004**, 16002, *108*

[19] Y.-W. Jun, S.-M. Lee, N.-J. Kang, J. W. Cheon, *J. Am. Chem. Soc.* **2001**, *123*, 5150

[20] a) L. Vegard, H. Schjelderup, *Phys. Z.* **1917**, *18*, 93. b) J. K. Furdyna, *J. Appl. Phys.* **1988**, *64*, R29. c) K. M. Hanif, R. W. Meulenberg, G. F. Strouse, *J. Am. Chem. Soc.* **2002**, *124*, 11 495. d) Y.-W. Jun, Y.-Y. Jung, J. W. Cheon, *J. Am. Chem. Soc.* **2002**, *124*, 615.

[21] S. K. Kulkarni, U. Winkler, N. Deshmukh, P. H. Borse, R. Fink, E. Umbach, *Appl. Surf. Sci.* **2001**, *169*, 438.

[22] M. V. R. Krishna, R. A. Friesner, *J. Chem. Phys.* **1991**, *95*, 8309.

[23] a) N. Pradhen, S. Efrima, *J. Phys. Chem. B* **2003**, *107*, 13 843. b) Y. C. Li, X. H. Li, C. H. Yang, Y. F. Li, *J. Mater. Chem.* **2003**, *13*, 2641.

[24] Y.-H. Kim, Y.-W. Jun, B.-H. Jun, S.-M. Lee, J. W. Cheon, *J. Am. Chem. Soc.* **2002**, *124*, 13 656.

[25] P. S. Nair, T. Radhakrishnan, N. Revaprasadu, G. Kolawole, P. O'Brien, *J. Mater. Chem.* **2002**, *12*, 2722.

[26] a) J. T. Hu, L. S. Li, W. D. Yang, L. Manna, L. W. Wang, A. P. Alivisatos, *Science* **2001**, *292*, 2060. b) L. S. Li, J. T. Hu, W. D. Yang, A. P. Alivisatos, *Nano. Lett.* **2001**, *1*, 349.

[27] D. V. Talapin, A. L. Rogach, A. Kornowski, M. Haase, H. Weller, *Nano. Lett.* **2001**, *1*, 207.

[28] L. H. Qu, X. G. Peng, *J. Am. Chem. Soc.* **2002**, *124*, 2049.

[29] C. M. Donega, S. G. Hickey, S. F. Wuister, D. Vanmaekelbergh, A. Meijerink, *J. Phys. Chem. B* **2003**, *107*, 489.

[30] D. V. Talapin, A. L. Rogach, E. V. Shevchenko, A. Kornowski, M. Haase, H. Weller, *J. Am. Chem. Soc.* **2002**, *124*, 5782.

FULL PAPERS

norganic Nanostructures

Y. C. Li, M. F. Ye, C. H. Yang, X. H. Li, Y. F. Li* ..... ■ – ■

Composition- and Shape-Controlled Synthesis and Optical Properties of $Zn_xCd_{1-x}S$ Alloyed Nanocrystals

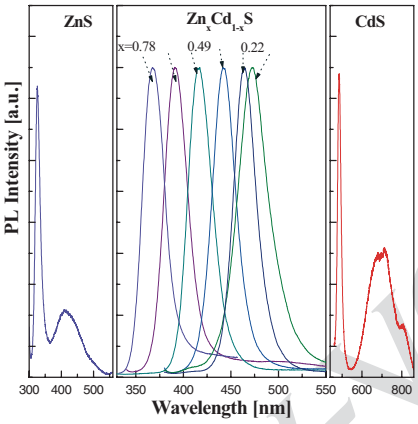

Composition-tunable ZnxCd1-xS alloyed nanocrystals are synthesized by thermolyzing the mixed cadmium ethylxanthate and zinc ethylxanthate precursors in a hot, mixed coordinating solvent. The nanocrystals formed show special composition-dependent optical properties (Photoluminescence is shown in the Figure). The shape-controlled synthesis of the nanocrystals is also realized by selecting appropriate ligand solvents.

